JOURNAL OF GEOPHYSICAL RESEARCH, VOL. 106, NO. A9, PAGES 19,081–19,099, SEPTEMBER 1, 2001

Plasma waves observed in the cusp turbulent boundary layer: An analysis of high time resolution wave and particle measurements from the Polar spacecraft

J. S. Pickett,[1] J. R. Franz,[2] J. D. Scudder,[1] J. D. Menietti,[1] D. A. Gurnett,[1]
G. B. Hospodarsky,[1] R. M. Braunger,[1] P. M. Kintner,[2] and W. S. Kŭrth[1]

Abstract. The boundary layer located in the cusp and adjacent to the magnetopause is a region that is quite turbulent and abundant with waves. The Polar spacecraft's orbit and sophisticated instrumentation are ideal for studying this region of space. Our analysis of the waveform data obtained in this turbulent boundary layer shows broadband magnetic noise extending up to a few kilohertz (but less than the electron cyclotron frequency); sinusoidal bursts (a few tenths of a second) of whistler mode waves at around a few tens of hertz, a few hundreds of hertz, and just below the electron cyclotron frequency; and bipolar pulses, interpreted as electron phase-space holes. In addition, bursts of electron cyclotron harmonic waves are occasionally observed with magnetic components. We show evidence of broadband electrostatic bursts covering a range of ~3 to ~25 kHz (near but less than the plasma frequency) occurring in packets modulated at the frequency of some of the whistler mode waves. On the basis of high time resolution particle data from the Polar HYDRA instrument, we show that these bursts are consistent with generation by the resistive medium instability. The most likely source of the whistler mode waves is the magnetic reconnection site closest to the spacecraft, since the waves are observed propagating both toward and away from the Earth, are bursty, which is often the case with reconnection, and do not fit on the theoretical cold plasma dispersion relation curve.

1. Introduction

The Polar spacecraft was launched in February 1996 into an approximate 1.8 by 9.0 R_E orbit with an inclination of ~86° and an orbit period of ~18 hours. This orbit was chosen so that Polar would initially have its apogee over the northern polar regions to provide an optimum platform from which to image the northern auroral oval and assess the energy deposited in the auroral region [*Acuna et al.*, 1995]. The Polar orbit has the added advantage that the spacecraft traverses the midaltitude to high-altitude northern cusp at radial distances of 7–9 R_E. As will be seen below, this was very fortuitous because it provided a means of studying the cusp and its boundary with the magnetopause with sophisticated instrumentation for extended periods of time. Since Polar is a part of the International Solar Terrestrial Physics (ISTP) program, in situ data from other spacecraft are available to provide velocity and density of the solar wind and the interplanetary magnetic field (IMF).

The polar cusp is the region of Earth in which magnetosheath plasma has direct access to the ionosphere [*Russell*, 2000] as shown in Figure 1. Because of this, the cusps are very important in the interaction of the solar wind with the magnetosphere [*Zhou et al.*, 1999] and exist whether the interplanetary magnetic field is northward or southward. Figure 1 shows the various regions surrounding the Earth in a plane perpendicular to the ecliptic plane with the Sun located to the left. The northern polar cusp, shown at the top of Figure 1, was sampled by Polar at high altitudes (~7–9 R_E) near its boundary with the magnetopause. This is the cusp region of interest in this paper because it is a very active region in terms of wave activity.

The focus of this paper is to present an overview of the waves that are observed in the turbulent boundary layer (TBL) of the cusp (which is pointed out in Figure 1 and which will be described in section 3), to discuss the mechanisms by which these waves may have been generated and to identify possible interactions of these waves with particles. Although wave and particle measurements have been made in the cusp and its boundary with the magnetopause for almost 30 years [cf. *D'Angelo et al.*, 1974; *Gurnett and Frank*, 1978; *Gurnett et al.*, 1979; *Klimov et al.*, 1986; *LaBelle and Treumann*, 1988; *Blecki et al.*, 1998], Polar's sophisticated instrumentation allows us to gain more information on these waves and particles and the processes associated with them. The primary advantage of the Polar instrumentation is the ability to capture all three components of both the electric and magnetic field waveforms simultaneously, which has never been done before in this region of space. The high time resolution particle measurements with sampling in three dimensions provide a means of comparing particle and wave energies in order to determine whether wave-particle interactions have taken place. We will begin by describing the instrumentation used in our study, followed by a description of the particular cusp region of interest. We then present the macroscale and microscale observations and an analysis of those observations, ending with a summary of our findings.

[1]Department of Physics and Astronomy, University of Iowa, Iowa City, Iowa.
[2]School of Electrical Engineering, Cornell University, Ithaca, New York.

Paper number 2000JA003012.
0148-0227/01/2000JA003012$09.00

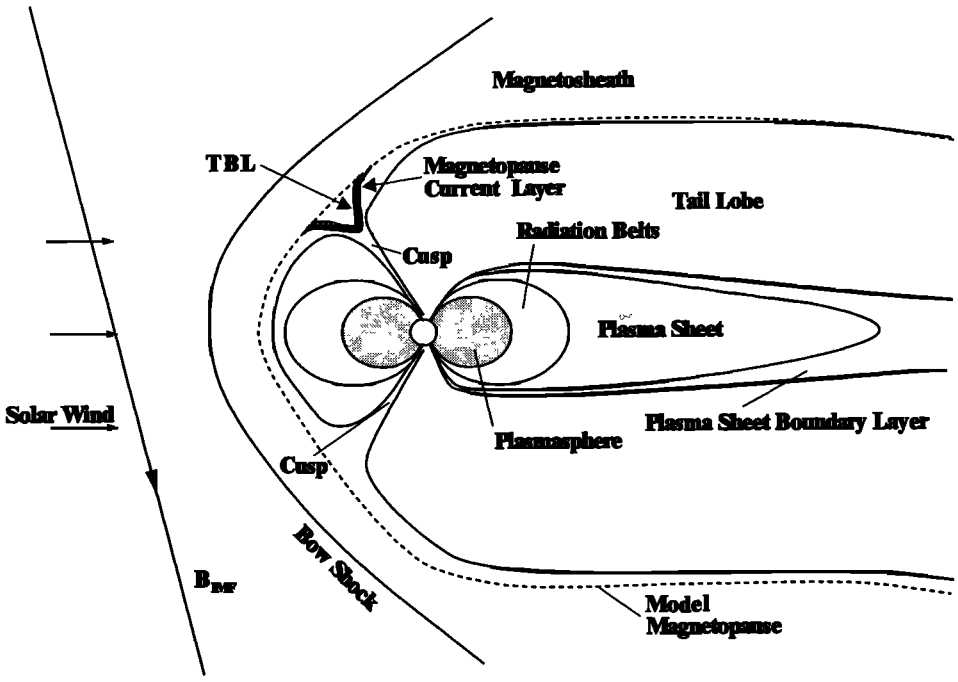

Figure 1. Schematic of Earth's magnetosphere and surrounding regions. The turbulent boundary layer (TBL) relative to the magnetopause current layer has been pointed out for the northern cusp. Although not shown, the southern cusp would contain a similar TBL.

2. Instrumentation and Data Reduction Techniques

The Polar spacecraft contains 13 instruments for measuring waves, fields, and particles and for imaging in the visible, ultraviolet, and X-ray frequency ranges [*Acuna et al.*, 1995]. Polar also contains a set of three orthogonal dipole antennas for measuring the DC and AC electric fields and a triaxial search coil for measuring AC magnetic fields (see Figure 1 of *Pickett et al.* [1999b] and description therein). In situ cusp TBL data will be presented in this paper from the following Polar instruments: plasma wave instrument (PWI) [*Gurnett et al.*, 1995]; HYDRA, a three-dimensional electron and ion hot plasma instrument [*Scudder et al.*, 1995]; and Magnetic Field Experiment (MFE) [*Russell et al.*, 1995].

PWI is composed of five receivers, three of which are used in this study, i.e., the Multichannel Analyzer (MCA) that samples in the frequency domain from 5.6 Hz to 311 kHz and the Low-Frequency Waveform Receiver (LFWR) and High-Frequency Waveform Receiver (HFWR) that capture waveform snapshots in the frequency range of 0.7–23 Hz and 20 Hz to 25 kHz, respectively. The HFWR also has an interferometry mode [see *Franz et al.*, 1998] for determining velocity and scale size. Refer to *Gurnett et al.* [1995] for a full description of these receivers. The HFWR and LFWR time series data were calibrated by performing a fast Fourier transform (FFT), applying the prelaunch-determined calibrations in the frequency domain, and then performing an inverse FFT back to the time domain. In the case of the LFWR magnetic field waveform data, an extra step is added after the forward FFT has been performed, i.e., multiplying the voltage of all frequency components by $2\pi f$ and then dividing all components by the calibration factor of VnT^{-1} at each frequency. This is done in order to conserve the waveform when the time series is recovered with the inverse FFT. If this extra step is not added, the low-frequency components will dominate the inverse FFT with the result that the high-frequency components will no longer be resolved. This low-frequency dominance is a consequence of the search coil calibration transfer function not being flat across the entire LFWR passband but rather being nearly linear, with positive slope, up to 10 Hz. The result of this extra calibration step for the LFWR results in the magnetic waveform data being presented in $nT\ s^{-1}$ rather than nT as expected from the $2\pi f$ multiplication factor applied in the frequency domain. This also means that there is no one function that will take the times series from $nT\ s^{-1}$ to nT. It is possible to do this for any one individual wave, though, by dividing the peak-to-peak value of the wave, in $nT\ s^{-1}$, by $2\pi f$, where f is the frequency of this wave.

The HYDRA instrument [*Scudder et al.*, 1995] is a suite of particle analyzers that provide three-dimensional measurements of the electrons and ions between ~2 eV q^{-1} and 35 keV q^{-1}, with a routine time resolution of 1.15 s. Full distribution functions of electrons and ions are determined from HYDRA data with a 13.8-s cadence (~2.3 rotations of the spacecraft) based on ion and electron energy sweeps on 12 separate detectors stepped simultaneously across the entire energy range in 1.15 s with ion sweeps interleaved between each of six electron sweeps. Electron density and temperature measurements are also available at 1.15-s resolution.

Since many of the waves observed in the cusp TBL occur in very short time interval bursts or pulses and are narrowband in frequency, we resort to using the minimum variance analysis (MVA) method [*Sonnerup and Cahill*, 1967] to determine the wave normal angle. We resolve the 180° ambiguity in the wave normal direction of whistler mode waves by checking the dot product of the Poynting vector (determined directly from the

wave fields **E** and **B** of the time series) with the wave normal vector since both vectors should have the same sign.

3. Turbulent Boundary Layer

The cusp turbulent boundary layer was distinguished as a distinct region of characteristic size 300–5000 km just outside and/or at the near-cusp magnetopause by *Savin et al.* [1998a] and by *Klimov et al.* [1986] using data obtained from the Interball 1 and Prognoz 10 satellites, respectively. Figure 1 shows the location of the cusp TBL with respect to the magnetopause current layer for the northern cusp. Although not shown in Figure 1, the southern cusp has the same configuration. Note that the magnetopause is deflected into the cusp by 1–2 R_E over that predicted by the model (Tsyganenko 89) magnetopause (dashed line) in the region of the cusp. According to *Savin et al.* [1998a], the TBL represents a permanent feature of the high-latitude magnetopause (including the near-tail magnetopause) and is not just confined to the cusp region, in which the maximum turbulence amplitudes are seen near the cusps. The TBL is best characterized by extreme magnetic turbulence and magnetic field vortices. Because of the rather permanent existence of the TBL, a substantial part of the reconnected field lines should cross the TBL in the vicinity of the cusp where the high level of turbulence makes them stochastic and randomizes the magnetosheath ions [*Savin et al.*, 1998b]. This scenario resembles the stochastic percolation model of *Kuznetsova and Zelenyi* [1990]. The turbulence would thus allow the cusp magnetic field lines to be disconnected from the magnetosheath with very different particle distributions just inside and outside the cusp-magnetosheath interface [*Savin et al.*, 1998b]. An example of a typical TBL crossing as observed by Polar will be presented in section 4.1.

4. Observations

4.1. Macroscale

Almost all of the observations presented in this paper were from the cusp TBL crossing of September 11, 1996, as shown in Plate 1. At ~0102 UT, Polar crossed the magnetopause current layer and entered the TBL at a radial distance of 8.8 R_E, a magnetic latitude of 66.6°, and a magnetic local time (MLT) of 1202 as it exited the polar cap. Polar remained in the TBL for over 2 1/2 hours, reentering the magnetosphere equatorward of the cusp at around 0333 UT at a distance of 7.4 R_E, a magnetic latitude of 45°, and a MLT of 1320.

An overview of some of the wave, field, and particle measurements made during a typical TBL crossing on September 11, 1996, is shown in Plate 1 as follows: (1) local magnetic field (from the DC-54 Hz data provided by MFE to HYDRA) (Plate 1a); (2) electron density obtained from the HYDRA instrument (Plate 1b); (3) wave magnetic field power spectral density covering the frequency range of 5.6 Hz to 10 kHz obtained from the PWI MCA (Plate 1c), with the white line showing the electron cyclotron frequency; (4) wave electric field power spectral density covering the frequency range from 5.6 Hz to 311 kHz obtained from the PWI MCA (Plate 1d), with the white line showing the electron cyclotron frequency obtained from MFE data; (5) electron differential energy flux covering the energy range from 10 eV to 20 keV from HYDRA (Plate 1e); and (6) ion differential energy flux covering the energy range from 10 eV to 20 keV from HYDRA (Plate 1f).

While Polar is in the TBL, the DC magnetic field is "noisy" as shown in Plate 1a, while the wave magnetic field as plotted in Plate 1c shows magnetic noise extending from 6 Hz, the lowest frequency measured, up to several hundreds of hertz. Plates 1a and 1b show that the overall magnetic field is depressed from ~60 to 20 nT, or ~70% reduction, while at the same time the density is enhanced from <1 cm^{-3} to ~10 cm^{-3} during the TBL crossing. The broadband electrostatic waves seen in Plate 1d extending from 6 Hz, the lowest frequency measured, up to a few tens of kilohertz are observed before, during, and after the TBL crossing but appear to be less intense across the entire frequency band outside the TBL and current layer. The auroral kilometric radiation (AKR) seen at frequencies greater than 100 kHz in Plate 1d is also present before, during, and after the TBL crossing. A few narrowband electromagnetic bursts are observed in Plate 1c around a few hundreds of hertz, as well as just below the electron cyclotron frequency. These bursts are almost always observed in the TBL region and are occasionally observed in the region just outside it.

The electron data in Plate 1e show enhanced fluxes in the TBL primarily in the range of 10 eV to 1 keV with occasional fluxes up to 10 keV. The most intense fluxes occur around 100 eV. Slightly reduced fluxes are seen in the region just outside and adjacent to the TBL. The ion data in Plate 1f show enhanced fluxes in the TBL primarily in the range of 40 eV to the highest measurement plotted, 20 keV. The most intense fluxes occur around 1–2 keV (which is typical for the cusp) in the TBL. Ion data from the Polar TIMAS instrument (not shown) reveal that in the TBL there are fluxes of both ionospheric and solar wind origin ions (W. Peterson, personal communication, 1999) as would be expected for the cusp. Since the ion data are more applicable to interactions involving waves at low frequencies in this region (<1 Hz, which is below the range of PWI), we will not comment further on them. The electron fluxes at lower energy and the anisotropy of the electrons will be discussed in section 5.

Although not shown in Plate 1, the TBL has the further characteristic that the particle pressure is greater than the magnetic pressure by up to a factor of 3–4. Analysis of the normal vector to the two TBL boundaries (0102 and 0333 UT) using the measured magnetic field and the method of *Sonnerup and Cahill* [1967] shows that the two smallest eigenvalues of the covariant matrix are almost equal. Thus the determination of the normal vector to the TBL boundaries using the magnetic field is inaccurate. We resort to transforming the magnetic field data into a boundary coordinate system, where **N** is normal to the boundary, **M** is tangent to the boundary and positive pointing toward dawn, and $\mathbf{L} = \mathbf{M} \times \mathbf{N}$. In doing so, we find that B_N nearly goes to zero at both TBL boundaries. Therefore these boundaries are nearly totally defined by the tangential components B_L and B_M, leading us to believe that at least for the September 11, 1996, event under review, the spacecraft encountered a discontinuity as it entered and exited the TBL. Because of the "noise" in the DC magnetic field data in the TBL, it is difficult to make this determination with certainty.

Figure 2 is an overview of the solar wind and IMF measurements made by the Wind spacecraft for the same 4-hour period as that for the Polar data in Plate 1. During this time, Wind was located ~5 R_E upstream from the bow shock of Earth and 16 R_E duskward of the Earth-Sun line at approximately (18 R_E, 16 R_E, 1 R_E) in GSE coordinates. Because of its close proximity to the Earth (delay time of ~1–2 min between Wind and Polar), Wind provides a good monitor of the solar wind

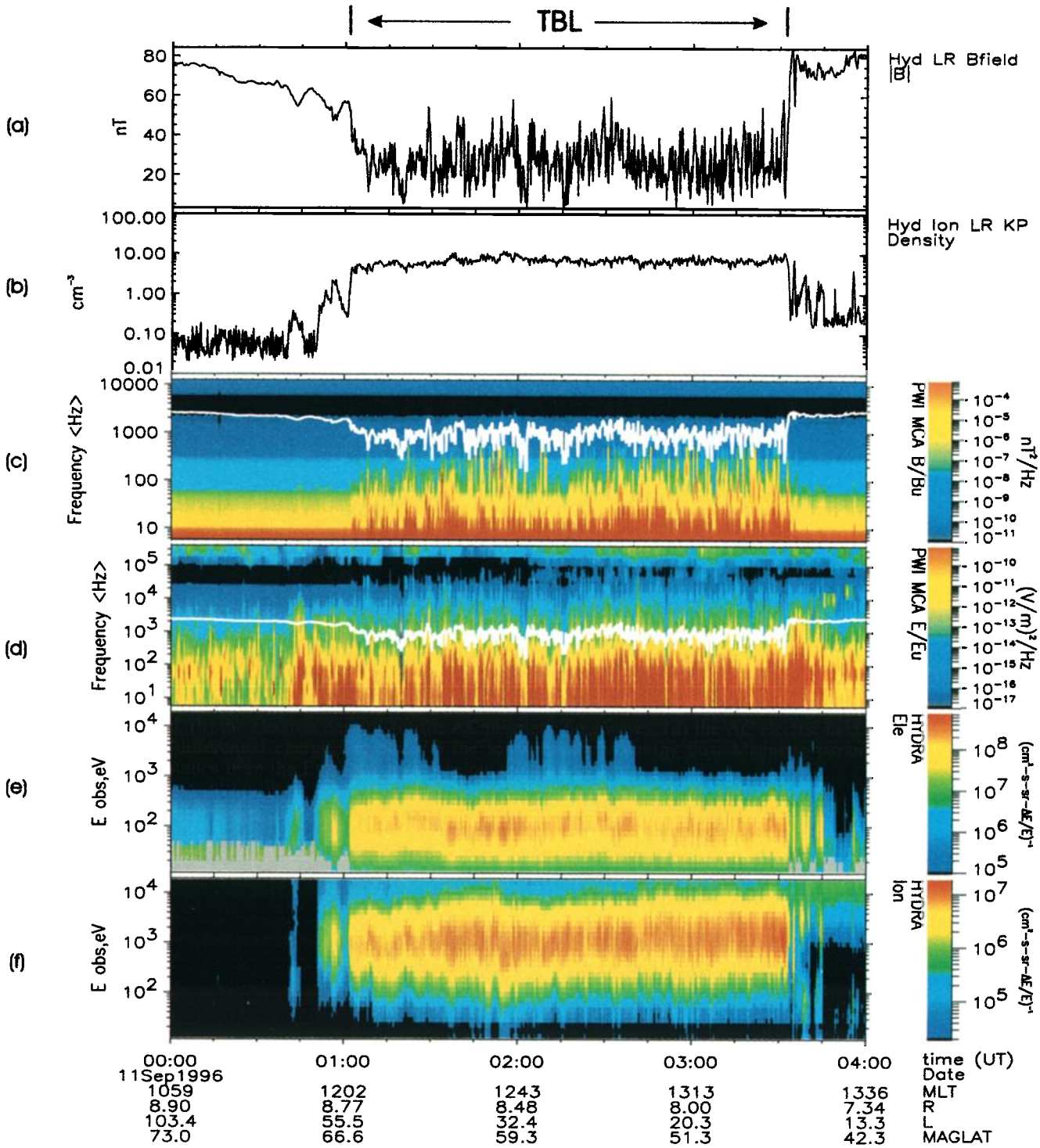

Plate 1. Four-hour plot of Polar data from September 11, 1996, from 0000 to 0400 UT, including (a) the magnetic field, (b) the electron density, (c) the AC magnetic field waves, (d) the AC electric field waves, (e) the electron differential energy flux, and (f) the ion differential energy flux. Magnetic parameters and spacecraft distance from the Earth are shown below the plots.

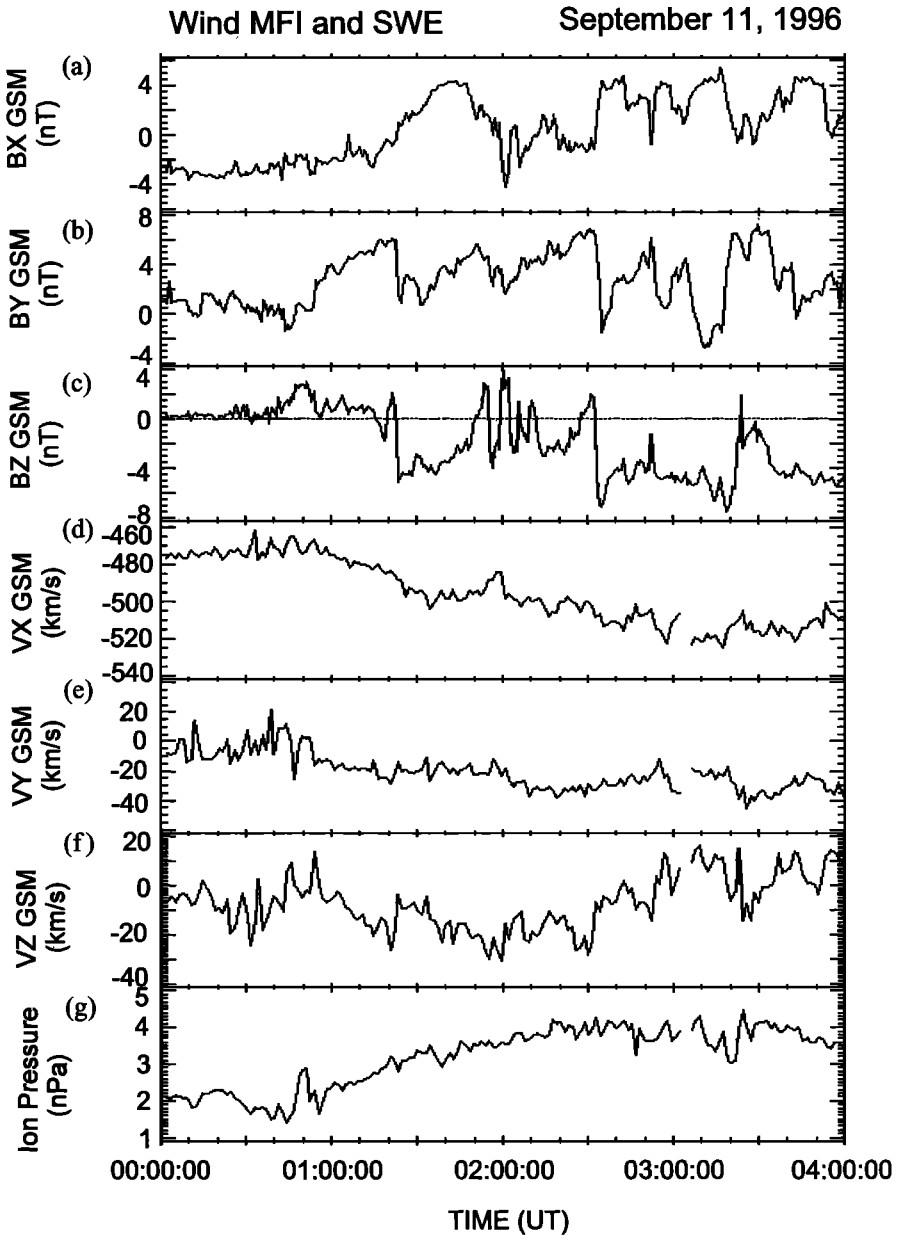

Figure 2. (a–g) Interplanetary magnetic field and solar wind data from the Wind spacecraft for the time period shown in Plate 1. Delay time from Wind to Polar is ~1–2 min. MFI, Magnetic Field Investigation; SWE, Solar Wind Experiment.

conditions at the nose of the bow shock. Figures 2a–2c are the *BX*, *BY*, and *BZ* components of the IMF in the GSM coordinate system, measured in nanoteslas. For the TBL crossing (~0102–0333 UT), the IMF *BZ* obtained from the Magnetic Field Investigation (MFI) instrument is almost zero until around 0120 UT. At that time it turns south and remains south for most of the TBL crossing with the exception of a period from ~0200 to 0230 UT, where it fluctuates between north and south. Note that the broadband magnetic noise observed in the TBL in Plate 1 appears to be slightly more intense during steady IMF *BZ* south.

Figures 2d–2f show the *X*, *Y*, and *Z* components of the solar wind velocity in the GSM coordinate system obtained by the Wind Solar Wind Experiment (SWE). The solar wind flow speed increases during almost the entire time that Polar is in the TBL, reaching a high of around 580 km s^{-1} by 0330 UT. This flow speed is elevated somewhat from a typical solar wind speed, with most of the flow directed along the *X* (Sun-Earth line) axis. The ion dynamic pressure is shown in Figure 2g. Although this pressure never gets very high, ~4 nPa maximum, the magnetopause current layer in the cusp appears to be sensitive to dynamic pressure changes as Polar seems to enter this layer just after the pressure pulse is observed in the pressure data at around 0047 UT. Polar is at ~8.8 R_E at this time, and the Tsyganenko 89 model would have predicted the current layer to be located at ~10 R_E. Thus the assertion by *Savin et al.* [1998a] that the magnetopause current layer is compressed into the cusp by 1–2 R_E further than its nominal position (as predicted by the Tsyganenko 89 model) appears to be accurate.

4.2. Microscale

As shown in section 4.1 with the Polar and Wind data, some aspects of the cusp TBL can be understood by analyzing the data of the region at the macroscale level. However, a great deal more can be learned about the region by examining the Polar wave data on the microscale level, data which for the first time have the time resolution and scope that are necessary to uncouple the various processes that are occurring almost continuously. In sections 4.2.1–4.2.3 we focus on the various waveform observations obtained by Polar PWI in the cusp TBL.

4.2.1. Electromagnetic waves. Two types of electromagnetic (em) waves are frequently observed in the cusp TBL: (1) AKR at frequencies of several tens of kilohertz to several hundreds of kilohertz and (2) bursts of electromagnetic waves at various frequencies, primarily around 15–25 Hz, 100–400 Hz, and just below the electron cyclotron frequency, f_{ce} (~400–1500 kHz). AKR is clearly visible in Plate 1d at frequencies >100 kHz prior to, during, and following the Polar spacecraft's traversal of the cusp TBL from ~0102 to 0333 UT. We will not elaborate any further on AKR, since it is known to be generated along the nighttime auroral field lines at radial distances of 2–4 R_E and to propagate to the cusp TBL with no identifiable particle interactions in the cusp TBL. The reader is referred to a review of auroral plasma waves by *Gurnett* [1991] for a discussion of the various characteristics of AKR.

Two bursts of em waves observed in the cusp TBL by the PWI LFWR on September 11, 1996, at ~0135:14 and 0135:16 UT are shown in Figure 3. The time series data covering 4.64 s beginning at 0135:13.257 UT have been transformed into a local DC magnetic field-aligned coordinate system. Figures 3a–3c are the three orthogonal electric field components in mV m^{-1} and Figures 3d–3f are the corresponding orthogonal magnetic field components in nT s^{-1}. The magnetic field data are plotted in nT s^{-1} rather than nT for the reasons outlined in section 2. The coordinate system is such that the Z component lies in the direction of the local DC magnetic field, the X component is chosen so that the radial vector outward from the center of the Earth to the spacecraft location, **R**, is in the meridian plane, and the Y component completes the right-handed coordinate system, being generally eastward. The data shown in Figure 3 were obtained at a radial distance of ~8.6 R_E, a MLT of 12.47, and a magnetic latitude of 62.45°. The electron cyclotron frequency during the burst at 0135:16 UT was around 230 Hz, the lower hybrid frequency was around 5.4 Hz, and the proton cyclotron frequency was around 0.13 Hz. This burst of em waves lasts for only ~0.6 s and is resolved clearly only in the magnetic channels, implying that the electric component falls at or lower than the background noise being picked up by the electric antennas. The largest component is that of the magnetic X component lying perpendicular to the DC magnetic field, $Bx_{\perp}$, and is about ±60 nT s^{-1} (or ~1 nT peak to peak). When the waveforms shown in Figure 3 are transformed to the frequency domain via a wavelet transform (not shown), we see that the bursts of em waves occur over a band from ~10 to 25 Hz with peak intensity around 18–19 Hz. Maximum power spectral density obtained from an FFT analysis is ~10^{-3} nT-rms^2 Hz^{-1}. Using the MVA method, we determined that the em burst shown in Figure 3 at ~0135:16 UT has a wave normal angle of ~141° with respect to **B** and is right-hand-polarized (determined by transforming the wave normal vector to a field-aligned coordinate system and checking the sign of its component along the field), thus identifying it as whistler mode since it falls below f_{ce} and above f_{LH} (lower hybrid frequency). We have examined several bursts in the cusp TBL similar to those in Figure 3 and found that they usually occur around 15–25 Hz, are right-hand-polarized, and have wave normal angles that fall within 20°–50° of **B**. In coming up with these values we have had to use some care because these bursts are almost never of constant amplitude or frequency, which is seen most clearly through wavelet analysis. Whistler mode waves at these low frequencies should be visible in Plate 1c in the MCA magnetic field data. Unfortunately, their amplitudes are low enough at these frequencies that they fall near the most intense part of the seemingly broadband magnetic noise and are most likely obscured for this reason in the MCA frequency domain data.

An overview of some of the other electromagnetic and electrostatic waves discussed below can clearly be seen in Plate 2 in the high time and frequency resolution plot of six consecutive snapshots beginning at 0136:04.892 UT on September 11, 1996. Plate 2 shows frequency versus time with color indicating power spectral density. Plates 2a–2c are the electric channels with frequency scale of 0–25 kHz (effective bandwidth), and Plates 2d–2f are the magnetic channels with frequency scale of 0–1.5 kHz. The coordinate system is the same field-aligned system discussed above. We have shown the abbreviated frequency scale for the magnetic channels since there is no other activity observable from 1.5 to 25 kHz. There are six consecutive 0.445-s snapshots from left to right, with the beginning of each snapshot being spaced 9.2 s apart. In order to get the full resolution of each snapshot, we have compressed the 8.755 s during which no data are being taken down to the very narrow, dark blue vertical lines seen between each snapshot.

Electromagnetic waves occurring around a few hundred hertz are clearly visible in the magnetic channels of the third snapshot in Plate 2. A portion of the HFWR waveforms associated with these waves is plotted in Figure 4 in the B-field-aligned coordinate system (the same coordinate system as that used in Figure 3 and Plate 2). This plot covers ~14 ms of time beginning at 0136:23.650 UT on September 11, 1996, when the spacecraft was at 8.6 R_E, MLT of 12.48, magnetic latitude of 62.31°, L of 39.69, and $f_{ce} \approx 1010$ Hz. The HFWR snapshot from which it was taken covered a total of 0.445 s and showed this particular wave packet lasting for only ~90 ms. Two other similar wave packets (not shown) are observed during the same 0.445-s snapshot. Thus it is clear that these waves do not occur continuously but occur in wave packets or bursts. They are often observed in the MCA magnetic field data (Plate 1c) as high-intensity bursts around a few hundred hertz over the broadband magnetic noise. Figures 4d–4f clearly show the waves occurring around 350 Hz based on the presence of five cycles of the wave over 14 ms. The maximum amplitude is seen in the $Bx_{\perp}$ component of around 0.05 nT peak to peak, and the minimum is seen in the $Bz_{//}$ component of around .02 nT peak to peak. Since we have not frequency-filtered these data, the electric field components of the 350-Hz waves are barely discernable, owing to the presence of other electrostatic emissions. When we filter the data so that only the 350-Hz em wave is observed, we find that the maximum amplitude of the electric field component perpendicular to **B** is ~0.04 mV m^{-1} and that parallel to **B** is ~0.1 mV m^{-1}. Using the MVA method on the time series of Figure 4 and filtering the data in the frequency range of 200–500 Hz, we obtain a wave normal angle of ~13° with respect to **B** as indicated in Figure 5. The left panel of Figure 5 shows the plane perpendicular to the wave normal

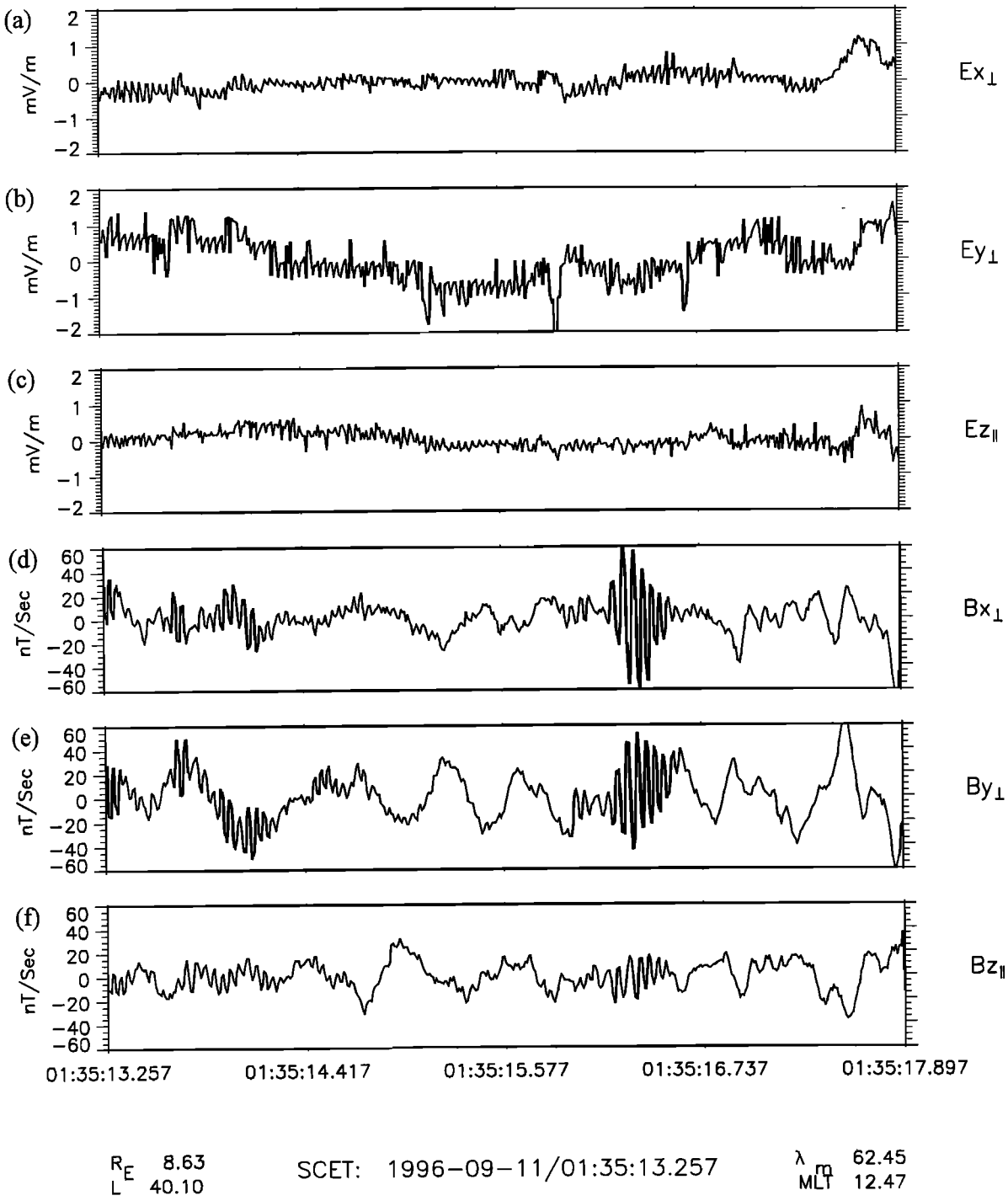

Figure 3. (a–f) A 4.64-s snapshot of the waveform recorded in all six channels simultaneously by the Low-Frequency Waveform Receiver showing two bursts of electromagnetic waves around 19 Hz.

angle, defined as the plane of polarization, with $B1$, the magnitude of the eigenvector corresponding to the largest eigenvalue, versus $B2$, the magnitude of the eigenvector corresponding to the middle eigenvalue. It shows that the waves are nearly circularly polarized (ellipticity equals 1/1.25). The middle and right panels show $B1$ versus the magnitude of the eigenvector corresponding to the smallest eigenvalue ($B3$, the component lying along the wave normal direction) and $B2$ versus $B3$, respectively. Both of these show that most of the field lies in the plane perpendicular to the wave normal direction, indicating that our analysis will be extremely reliable. Transforming the wave normal vector into a local magnetic field-aligned coordinate system and checking the sign of its component along the field provides us with the further information that these waves are right-hand-polarized. Further, because they lie between f_{ce} and f_{LH}, they are identified as whistler mode waves. Figures 4a–4f show that the amplitude of these waves is also changing slightly over time, in this case, of

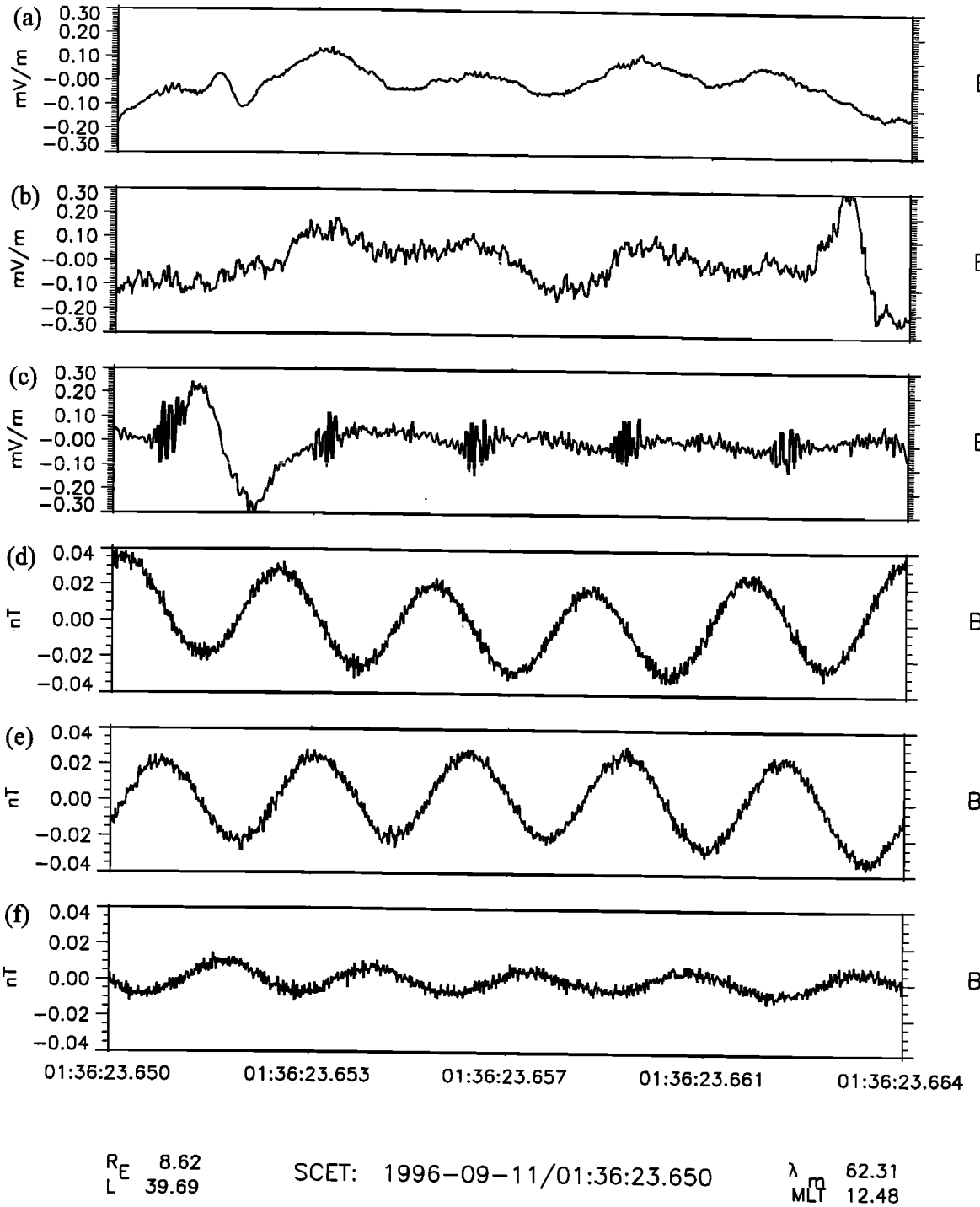

Figure 4. (a–f) A 14-ms plot of the waveforms seen in all channels of the Polar PWI High-Frequency Waveform Receiver showing an electromagnetic wave around 350 Hz and electrostatic bursts in packets at the 350-Hz frequency.

five cycles of the wave, but the change is not significant enough to affect the analysis.

Of particular interest in Figure 4 are the electrostatic (es) bursts occurring primarily along **B** and which are observed in the spectrogram of Plate 2 as broadband electrostatic waves. We will not discuss the large electrostatic pulses (~−.30 to +.30 mV m^{-1}) observed along $Ez_{//}$ immediately following the first es burst and along $Ey_{\perp}$ at the end of the plot except to say that we suspect that they are a type of potential structure, perhaps an electron hole (see section 4.2.2 for a discussion of electron phase-space holes). In Figure 4 the es bursts, or wave packets, are modulated at the frequency of the 350-Hz whistler mode wave burst just discussed above. The electric field amplitude of these bursts varies from around 0.06 to 0.10 mV m^{-1}. The frequency of the es waves within the wave packet is continuously changing with time as shown by wavelet analysis.

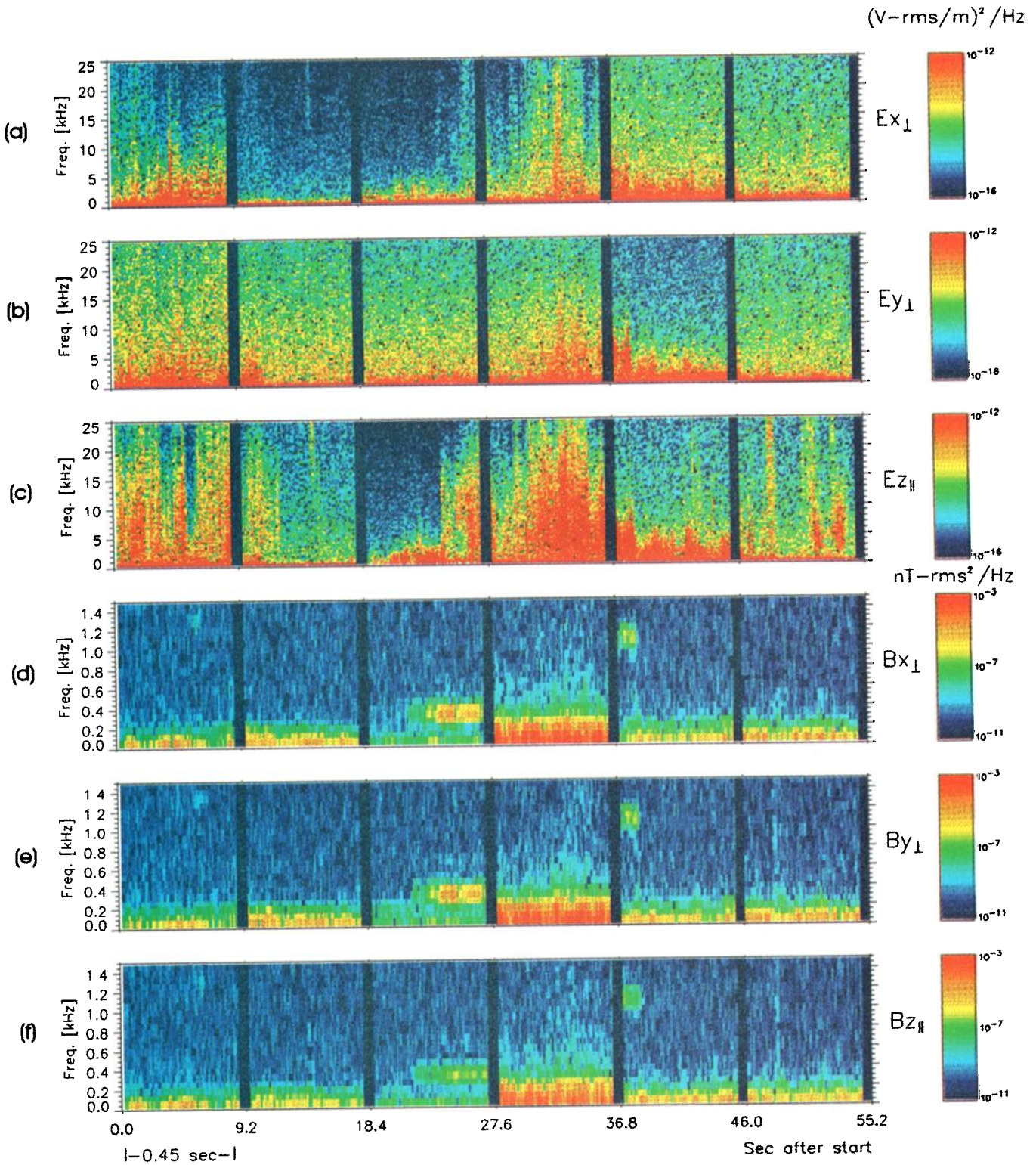

Plate 2. (a–f) Six consecutive snapshots of the spectrograms obtained from the waveforms recorded by the six channels of the Polar PWI High-Frequency Waveform Receiver. Color indicates power spectral density. Various electrostatic and electromagnetic emissions are seen during this ~1 min of data presented in a magnetic field-aligned coordinate system. Each snapshot covers 0.445 s with the intervening dark blue vertical lines representing 8.755 s of compressed time.

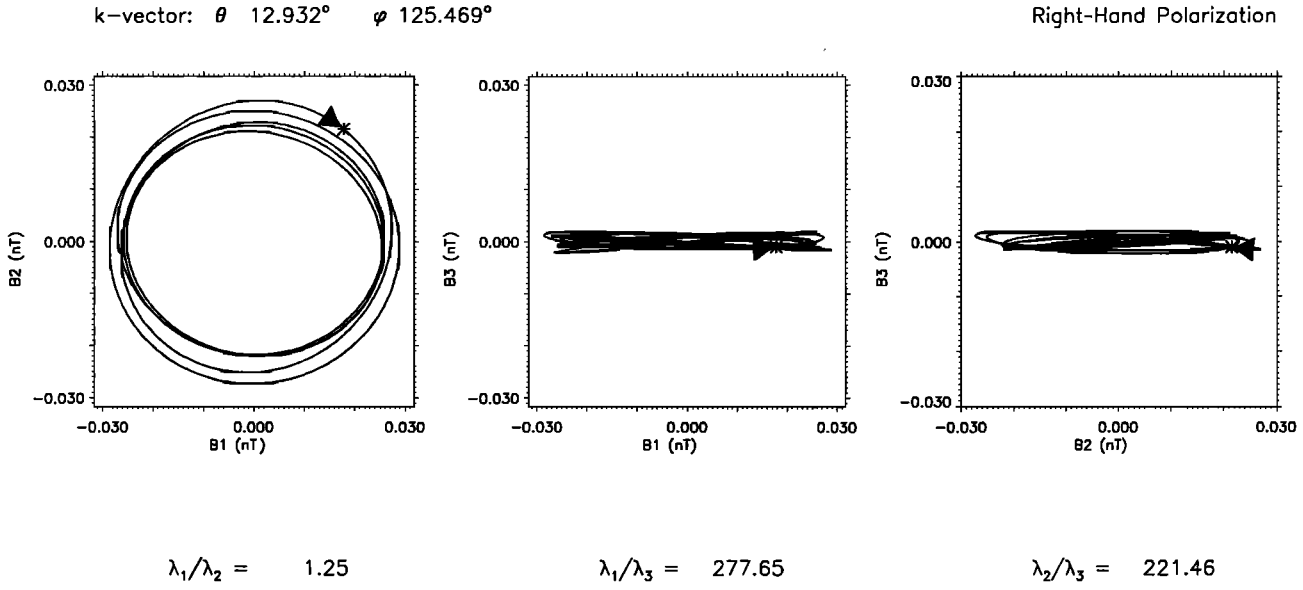

Figure 5. Minimum variance analysis of the 350-Hz electromagnetic wave seen in Figure 4, showing that the wave is circularly polarized with a wave normal angle of ~13°.

Thus the es bursts appear as a broad band in the frequency range of ~2–20 kHz with peak power around 8–12 kHz, which is below the plasma frequency of ~28 kHz based on HYDRA electron data and above the electron cyclotron frequency of ~1 kHz. There does not appear to be a magnetic component to these bursts, or if there is, it is below the noise floor of the receiver. Even though the most intense wave packets are modulated at the frequency of the 350-Hz wave, there is some indication that these electrostatic emissions are occurring almost continuously. Note the less intense emissions at around the same frequency between the intense bursts in Figure 4. In fact, during the 14 ms following the time period in Figure 4, these es waves are seen almost continuously at nearly constant intensity, rather than in wave packets at the whistler mode frequency.

Interferometry measurements obtained during a similar cusp TBL on September 22, 1996, also show the presence of a low-frequency (few hundred hertz) wave with es bursts at kilohertz frequencies modulated at the frequency of the lower-frequency wave [*Franz*, 2000]. In interferometry mode, one-half of the electric V, spin plane, antenna (between one sphere and the spacecraft body, ~50 m) is biased positive (EV+), and the other half is biased negative (EV−). Interferometry data are plotted in Figure 6 as follows: Figures 6a and 6b are the 110 ms of the EV+ and EV− waveforms, respectively; Figures 6c and 6d are the power spectral density (PSD) versus frequency of these waveforms; Figure 6e is the coherence of the two waveforms versus frequency; and Figure 6f is the phase shift versus frequency obtained from the cross spectrum when the correlation is >0.80. In this analysis, sixteen 512-point FFTs have been averaged to estimate the spectra and cross-spectra. During the time period shown in Figure 6 a nearly continuous wave around 300 Hz and bursts of wave power in a band from 3 to 25 kHz (the upper band limit) are observed (see Figures 6c and 6d). The high-frequency waves might be Langmuir waves since the plasma frequency at this time is around 19 kHz based on Polar HYDRA density measurements. The waveform data in Figures 6a and 6b clearly show the ~300 Hz wave with electrostatic bursts occurring at a fixed phase of the 300-Hz wave. Both of these emissions are seen at about the same frequencies as those observed by the six-channel waveform receiver 11 days earlier, as shown in Figure 4, and are typical emissions in the cusp TBL. Thus the 300-Hz wave observed in the interferometry mode is interpreted to be a whistler mode wave with a wave normal angle >0°. Cross-spectral analysis [see *LaBelle and Kintner*, 1989] (Figure 6f) shows that for the frequencies between 3 and 25 kHz comprising the electrostatic bursts, the coherence is greater than 0.9, and the phase shift between the two channels has a linear slope, indicating that all of the frequencies have the same phase velocity. Since we chose our analysis interval during a time when the V antenna was nearly parallel to **Bo**, we obtain a phase velocity for these electrostatic bursts of 3400 km s^{-1} parallel to **Bo**.

Electromagnetic waves that occur just below or at the electron cyclotron frequency are commonly observed in the cusp TBL. A 29-ms interval of the field-aligned time series of these waves beginning at 0136:41.749 on September 11, 1996, is shown in Figure 7 and observed in the spectrogram of Plate 2 at the beginning of the fifth snapshot. At this time, f_{ce} = 1220 Hz, and the spacecraft is located at 8.62 R_E, with MLT of 12.48, magnetic latitude of 62.27°, and L of 39.58. The wave can be seen best in Figures 7d–7f (magnetic field channels). Near the end of the plot this wave burst disappears, the entire em burst occurring over ~90 ms. An electrostatic burst similar to those just described in Figure 4 is seen at ~0136:41.75 UT in Figure 7, but the wave packet is obviously not occurring at the frequency of the em wave just below f_{ce}, nor is it occurring at a frequency around 350 Hz. On the basis of the waveform data before the start of Figure 7, the es bursts appear to be occurring at a much lower frequency around 20 Hz, which is consistent with the 19-Hz electromagnetic wave described above and which is seen in the LFWR. Unfortunately, LFWR and HFWR data can never be sampled simultaneously, owing to memory constraints. The wave normal angle of the em wave shown in Figure 7 is 8.3°, and it is right-hand-polarized. Thus it too is probably a whistler mode wave since its frequency is

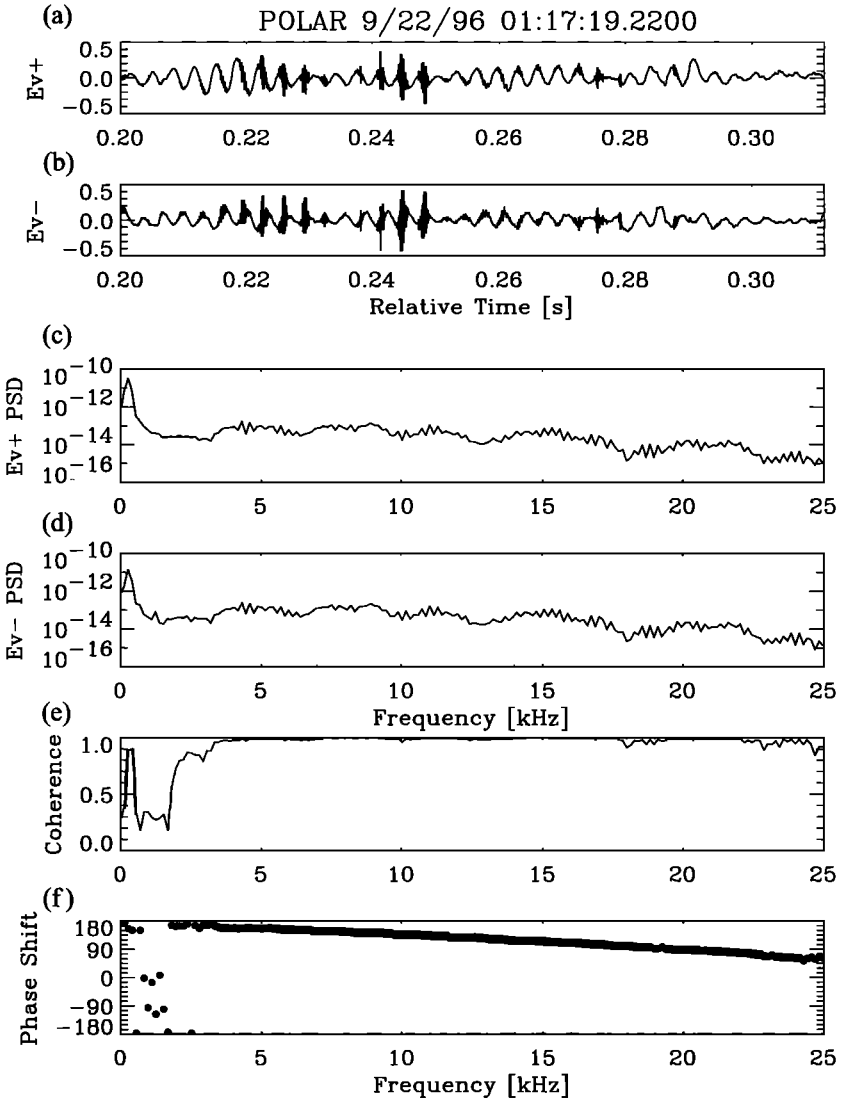

Figure 6. (a–f) A 14-ms plot of the waveforms seen in all channels of the High-Frequency Waveform Receiver, showing an electromagnetic wave around 350 Hz and electrostatic bursts in packets at the 350-Hz frequency.

around 1150 Hz and the electron cyclotron frequency is around 1220 Hz. The frequency of the electrostatic burst is ~2.5 kHz, but it changes slightly throughout the wave packet as does the previous es burst example. The em waves just below f_{ce} and shown in Figure 7 are typical for the cusp TBL.

4.2.2. Electron phase-space holes. Electron phase-space holes, observed by the Polar PWI interferometer as bipolar pulses in the electric field waveform data throughout much of its orbit, have been extensively studied by *Franz et al.* [1998, 2000] and *Franz* [2000]. This research shows that electron phase-space holes are inferred in the cusp with velocities along **Bo** of a few hundred to 1000 km s^{-1} and parallel to perpendicular size of <0.45. In relation to the holes observed in the plasma sheet, the cusp holes are traveling slower and are more pancake-like. These results are similar to those obtained by *Cattell et al.* [1999]. The velocities of the electron holes are determined by the lag time between the detection of the structure at one sphere of the EV antenna and its detection by the other half of the EV antenna [*Franz et al.*, 1998]. Typical examples of the bipolar pulses observed in the PWI waveform data are found in the work of *Franz et al.* [1998, 2000] and *Franz* [2000] and thus will not be presented here. We note, however, that in the cusp TBL these structures are moving both parallel and antiparallel to the local magnetic field. As pointed out in section 4.2.1, the bipolar signatures observed in Figure 4 may be similar potential structures.

4.2.3. Electron cyclotron harmonic waves. For completeness, we note the presence of electron cyclotron harmonic (ECH) waves throughout the TBL crossing. These waves were discussed briefly by *Pickett et al.* [1999a]. Although these waves have been observed in the cusp by several other spacecraft, Polar PWI provided the first six-channel, high time/frequency resolution measurements of the waveforms. The waves are occasionally observed to have magnetic components at the fundamental frequency and at one or two harmonics [see *Pickett et al.*, 1999a, Figure 2a]. A short burst of these waves is also seen in the spectrogram of Plate 2 near the end of the first snapshot, where the harmonics are observed in the electric channels and the fundamental is observed in the magnetic channels around 1.3 kHz. Figure 8 shows a 14-ms sample of a

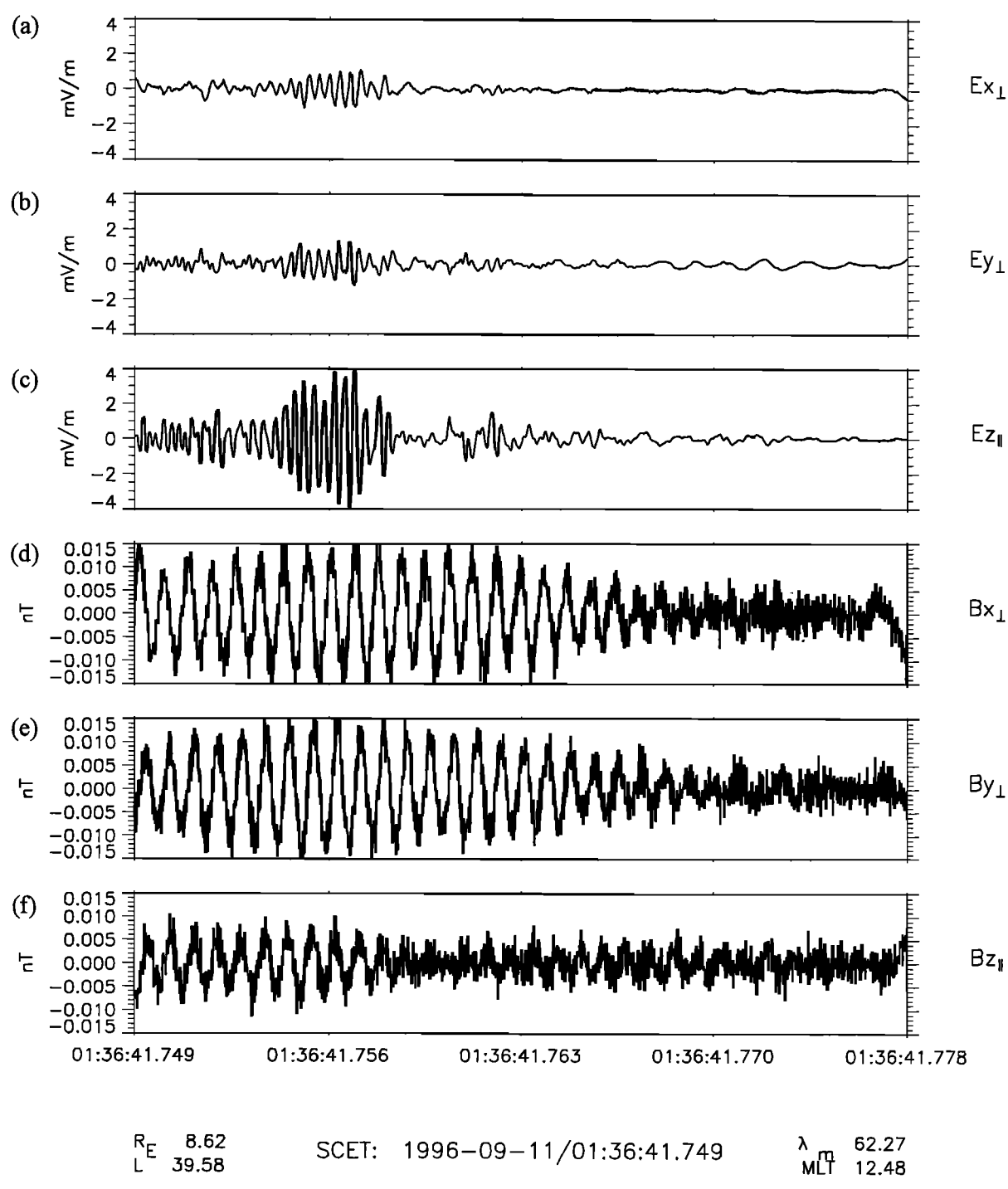

Figure 7. (a–f) A 29-ms sample of waveform data from the High-Frequency Waveform Receiver showing an electromagnetic wave at ~1150 Hz and an electrostatic burst at a frequency of ~2200 Hz.

typical ECH waveform beginning at 0152:01.764 UT on September 11, 1996, from the HFWR with the three electric components (Figures 8a–8c) and the three magnetic components (Figures 8d–8f) in a local B-field-aligned coordinate system. These data have not been filtered, since it would be difficult to filter out waves falling outside the range of the ECH waves, which have harmonics up to the highest frequency of the receiver. In Figure 8 we observe that most of the wave electric field is contained in the plane perpendicular to the local magnetic field. Using the MVA method and the three magnetic components to obtain the k vector, we have found that the wave normal angle generally falls in the range of 82°–86°. When using the electric vectors to obtain polarization for the fundamental frequency of around 1.1 kHz ($f_{ce} \approx 952$ Hz), we find that we obtain both left- and right-handed polarizations. Figure 9 shows the polarization for the waveform plotted in

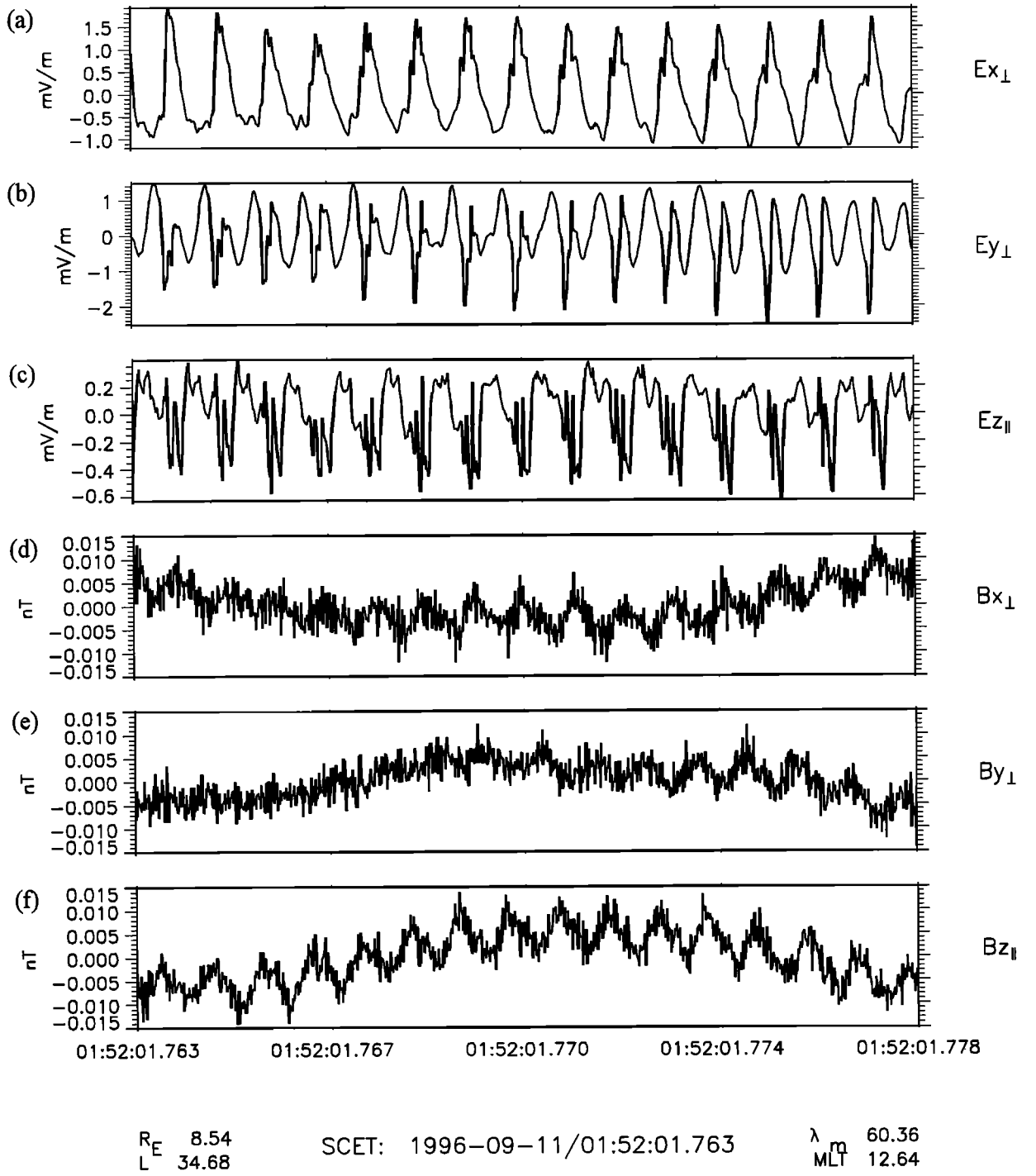

Figure 8. (a–f) A 14-ms sample of waveform data from the High-Frequency Waveform Receiver showing electron cyclotron harmonic waves, including a magnetic component at the fundamental and first harmonic.

Figure 8. Here we have taken the electric field measurements and put them in a B-field-aligned coordinate system, calculated the total wave electric field in this filter passband at each sample, and normalized each of the field-aligned components to this value. Figure 9a shows the plane perpendicular to **B**, and Figures 9b and 9c show the other two planes, both of which contain the direction of **B**. This particular plot shows a left-handed wave, whereas a plot of the prior snapshot showed a right-handed polarization. The implications of this result are still under investigation. Although the ECH waves sometimes have a small magnetic component, this is merely an indication that the electrostatic criteria ($k_\perp$ sufficiently large) are not fully satisfied, as per *Stix* [1992], but nearly so as to give an index of refraction that would suggest that the waves are electrostatic [*Pickett et al.*, 1999a]. The ECH waves measured by the Polar HFWR in the polar cap have similar characteristics with respect to polarization and are the subject of a study by *Menietti et al.* [2001].

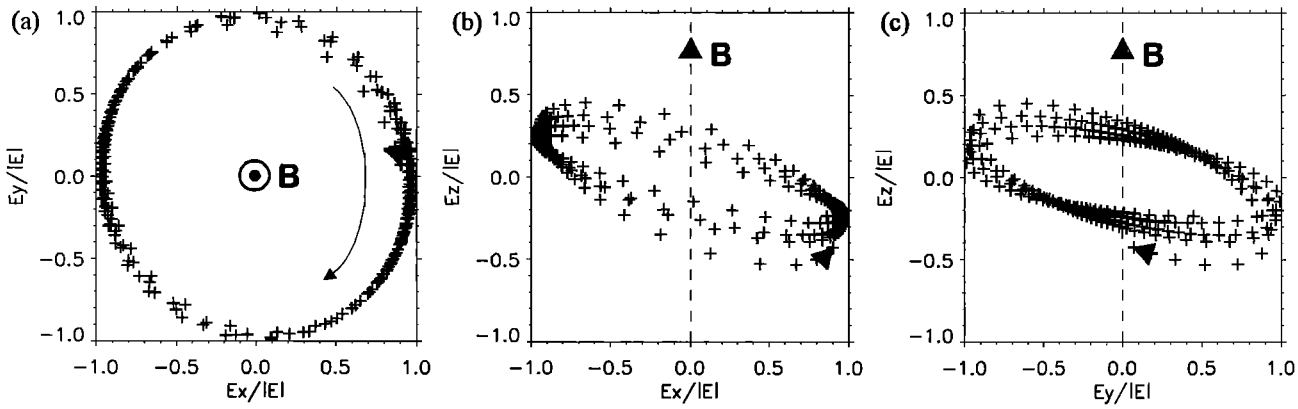

Figure 9. (a–c) Polarization of the electron cyclotron harmonic waves shown in Figure 8 showing left-hand polarization. A plot from the previous 14 ms shows right-hand polarization.

5. Discussion

The few tens of hertz, few hundreds of hertz, and just below f_{ce} whistler mode waves are being definitively identified and characterized for the first time in this cusp TBL region primarily because of the high time and frequency resolution of the Polar PWI data. Previously, most wave measurements were obtained directly in the frequency domain or in the time domain in one direction only. Polar PWI provides wave measurements in all three orthogonal directions of **E** and **B** simultaneously. The short whistler mode bursts (a few milliseconds) were not well resolved in the spectrograms, because they were detected at the same time and in the same frequency range as the intense broadband em turbulence. In instruments such as the sweep frequency receivers, which take several seconds to sweep the lower frequency ranges, the short bursts tend to get averaged out by the more intense turbulence. The PWI MCA is able to detect them because it takes a spectrum every 1.3 s, providing a greater opportunity to observe a short burst whistler mode wave without the presence of a burst of turbulence. The waveforms obtained in the cusp TBL clearly show the presence of turbulence, which appears nonsinusoidal with random amplitudes in the time domain, and whistler mode waves, which are more or less sinusoidal, and provide the opportunity to find selected periods where the two are not occurring at the same time.

The whistler mode waves around 100–400 Hz observed in the cusp TBL are very similar to lion roars ($f \approx 100$ Hz, typical amplitude of 0.1 nT, and an average burst duration of 1–2 s) that are observed in the magnetosheath [*Smith and Tsurutani*, 1976] and which are believed to be excited by a cyclotron instability with anisotropic magnetosheath electrons [*Thorne and Tsurutani*, 1981]. Many of the lion roars are reported to be observed during times when the magnetic field and plasma density are out of phase with each other, the magnetic field being depressed and the density being enhanced. The TBL as a whole has this characteristic, but when we look at the individual whistler mode wave bursts occurring on short timescales, this is not the case. We now investigate whether an electron flux anisotropy is sufficient to generate the whistler mode waves in the cusp TBL. When the whistler mode waves described above are observed at 0135–0137 UT at frequencies around 19 Hz, 350 Hz, and just below f_{ce} at 1150 Hz, their measured phase velocities along **B**, V_{ph}, are as shown in Table 1 and calculated as follows:

$$V_{ph} = (|d\mathbf{E}|/|d\mathbf{B}|) \cos \theta, \tag{1}$$

where $|d\mathbf{E}|$ and $|d\mathbf{B}|$ are calculated from the three orthogonal wave electric and magnetic field measurements (as in Figure 4, for example) and θ, the wave normal angle, is calculated by the MVA method (as in Figure 5, for example). For comparison, Table 1 also shows the phase velocities of these waves using the cold plasma dispersion relation for whistler mode waves traveling along B calculated as follows:

$$v_\omega = c\{1 + \omega_{pe}^2/[\omega(\Omega_{ce} \cos \theta - \omega)]\}^{-1/2}, \tag{2}$$

where c is the speed of light, ω_{pe} is the plasma frequency, Ω_{ce} is the electron cyclotron frequency, and ω is the frequency of the whistler mode wave. Table 1 shows that the expected values of V_{ph} are quite different from the measured values of V_{ph} for all of the whistler mode waves listed. In particular, the whistler

Table 1. Frequencies of Characteristic Whistler Mode Waves in the Cusp TBL and Associated Plasma Parameters[a]

Frequency, Hz	Measured E/B, km s^{-1}	Measured θ, deg	Measured V_{ph} From Equation (1), km s^{-1}	Measured f_{ce}, Hz	Measured f_{pe}, Hz	Theoretical V_{ph} From Equation (2), km s^{-1}	$E_{//R}$ Opposed From Equation (3), eV	$E_{//R}$ Aligned From Equation (3), eV
19	≤1,500	141	≤1,166	230	28,460	581	663	480
350	3,333	13	3,248	1,010	28,460	4,966	452	107
1,150	20,000	8.3	19,791	1,220	28,460	2,703	4,730	4

[a]Parameter θ is the wave normal angle, V_{ph} is the phase velocity of the wave along **B**, f_{ce} is the electron cyclotron frequency, f_{pe} is the electron plasma frequency, and $E_{//R}$ opposed and $E_{//R}$ aligned are the parallel resonant electron energies corresponding to these waves traveling in the opposite and same directions, respectively, as the electrons.

mode wave just below f_{ce} at 1150 Hz has a phase velocity that is an order of magnitude higher than the theoretical value for a cold plasma. Although the measured value of the electron plasma density used in calculating ω_{pe} in (2) has some error associated with it, this error would not be sufficient to explain the difference between the measured V_{ph} and the theoretical one using the cold plasma dispersion relation. This probably implies that the plasma is warm and that the dispersion relation needs to be modified to take this into account. Because of this variance, we have chosen to use the measured values of V_{ph} when calculating the resonant energy. Using (7) of *Tsurutani and Lakhina* [1997], the parallel kinetic energy of resonant electrons can be written as

$$E_{//R} = 1/2 m_e V_{ph}^2 (1 - \Omega_{ce}/\omega)^2, \quad (3)$$

where m_e is the electron mass, V_{ph} is the parallel phase speed of the wave calculated according to (1), Ω_{ce} is the electron cyclotron frequency, and ω is the frequency of the wave for which V_{ph} was calculated. Table 1 shows the calculated values of $E_{//R}$ for electrons traveling in the opposite and same directions as the waves. These electron energies appear to fall within the range of energies for which there are significant differential energy fluxes that could cause the cyclotron instability to take place. Figure 10 is a plot of electron temperature anisotropy, $A^e = T_{e//}/T_{e\perp}$, which covers the time period during which the whistler mode waves discussed in Figures 4 and 7 were observed. Figure 10 clearly shows that during this time, $A^e > 1$. Thus we can rule out that these whistler mode waves were generated locally by a cyclotron instability at the exact time they were observed, since this instability requires $A^e < 1$. However, A^e in the cusp TBL is often <1, as shown in Figure 10, allowing for the possibility that these whistler mode waves were generated elsewhere in the TBL but observed by the spacecraft as they propagated away from the generation site. If this is the case, a certain percentage of them should be observed during times of $A^e < 1$. This would require a statistical study, as well as an investigation of the behavior of the cyclotron instability in a warm plasma such as we have shown may be the case in the cusp TBL, which is beyond the present scope of this paper. It is reasonable to expect that the whistler mode waves just below f_{ce} could possibly be auroral hiss that has propagated to the cusp TBL, since their frequencies around 1 kHz are typical of hiss. *Gurnett and Frank* [1978] report the observation of auroral hiss at high altitudes in the cusp, $R > 6$ R_E. However, auroral hiss is usually not found to be as bursty as these whistler mode waves in the cusp TBL. In addition, the low-frequency whistler mode waves could have been generated at the bow shock or in the magnetosheath as lion roars and propagated to the cusp, since both types of waves have similar characteristics. However, we feel that a stronger possibility for the generation mechanism of the few hundred and few tens of hertz whistler mode waves, as well as the electromagnetic turbulence that is observed up to f_{ce}, might be one which involves reconnection, since the whistler mode waves are seen propagating both toward and away from the Earth and these waves and the turbulence are bursty, which is often a characteristic of certain types of magnetic reconnection. *Drake* [1995] states that the current layer driven at the X line during magnetic reconnection has a transverse scale length of the order of or smaller than the electron skin depth, c/ω_{pe}, which means it is quite narrow. In three-dimensional (3-D) simulations, such current layers are strongly unstable to current gradient-driven whistlers and evolve into a turbulent state consisting of filamentary, finite-length streams of electrons, embedded in a broader current layer. The electromagnetic fluctuations associated with this turbulent current layer are broadband, extending up to the f_{ce}, with embedded peaks, and are composed of kinetic Alfven and whistler modes [see also *Mandt et al.*, 1994; *Gekelman and Stenzel*, 1984]. The Polar wave observations in the cusp TBL (whistler mode waves and electromagnetic turbulence up to f_{ce}) fit this proposed description of the reconnection outflow (or exhaust) region quite well. Whether the Polar spacecraft is located in the outflow region of a localized reconnection site or several R_E away from its accepted reconnection site at the subsolar point (for southward IMF) along reconnected field lines that pass through the cusp TBL is still to be determined. Current studies of whistler mode waves and turbulence observed at a recently identified reconnection site with Polar data should give us the answers in the near future.

Given that the whistler mode waves are always present when the electrostatic bursts are generated and that they are sometimes modulated at the whistler mode frequency, we look for a generation mechanism for these bursts that involves both emissions. Such a mechanism was described by *Reinleitner et al.* [1983] and *Gurnett and Reinleitner* [1983] in connection with electrostatic waves observed on ISEE 1 and ISEE 2 in association with whistler mode chorus waves near the equatorial magnetopause. The whistler mode chorus observed in *Reinleitner et al.*'s [1983] study ranged from 100 to 800 Hz, and the electrostatic bursts were normally in the range 3 up to 10 kHz, which was usually somewhat lower than the electron plasma frequency. The wave vectors of the electrostatic bursts were field-aligned. All wave measurements were made in one direction only, so that some assumptions had to be made in determining various parameters in this study, which is not the case with the Polar measurements. Applying the mechanism described by *Reinleitner et al.* [1983] to our case, we note that the whistler mode waves around 350 Hz have an electric component parallel to the magnetic field since the wave normal angle is around 13°. This parallel component at 350 Hz (velocity approximately 3.25×10^3 km s^{-1} and electric field intensity approximately 0.1 mV m^{-1}) has a wavelength $\lambda = V_{//ph}/f \approx$ 9300 m, which provides a potential well of 9300 m × 0.1 mV m^{-1} = 0.93 V. This should provide enough of a potential well to be able to trap electrons at ~30 eV that are in Landau resonance with the whistler waves, since the equivalent electron energy of the whistler mode wave is ~30 eV ($E = 1/2\, m_e V_{//ph}^2$). A field-aligned electron beam at ~30 eV is observed at the same time as the ~350 Hz whistler mode wave (see Figure 11). Once the electrons are trapped, they become spatially bunched near the minimum in the effective potential well produced by the parallel electric field of the whistler mode wave. The spatial bunching explains why the electrostatic bursts would occur in discrete packets in phase with the whistler mode wave. Each bunch of trapped electrons could then excite a burst of electrostatic noise via a two-stream instability. Just as in the case of *Reinleitner et al.* [1983], the resistive medium instability, which is a type of modified two-stream instability, is the most likely candidate for explaining the observations, since it would result in a downshift in frequency of the electrostatic bursts below the local plasma frequency as measured. The instability is applicable only in the regime where V_o/V_T is on the order of 1, where V_o is the velocity of the beam and V_T is the average thermal velocity of the plasma electrons. In our case, $V_o \approx$ 30 eV, and V_T is ~40 eV. Since the instability requires Landau damping to operate, the beam velocity must

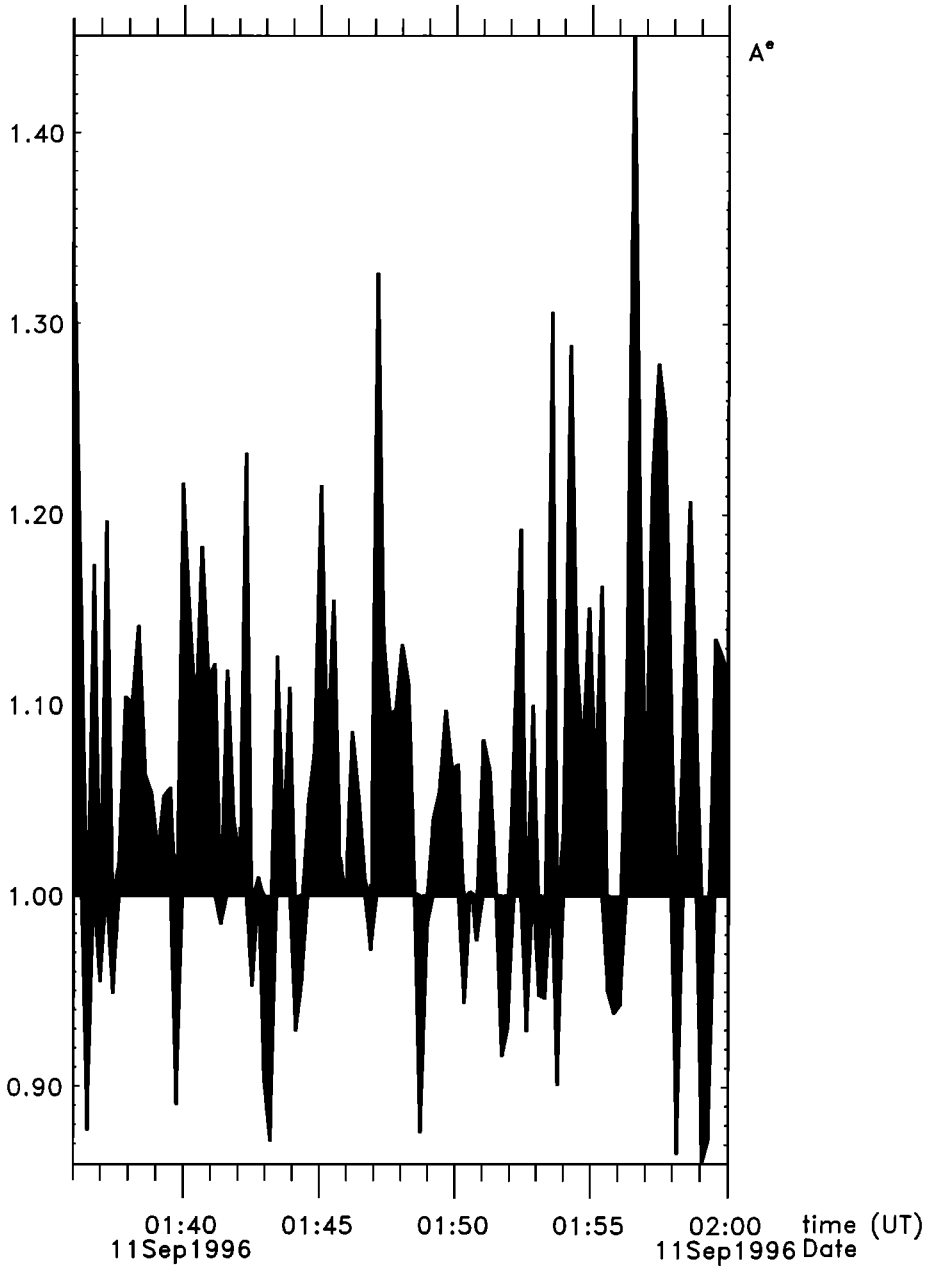

Figure 10. HYDRA electron anisotropy data, A^e, where A^e is the ratio of the parallel electron temperature to the perpendicular electron temperature for the time period that includes the waveform data shown in Figures 4, 7, and 8.

be in the region of steep slope on the electron distribution function, which it is, rather than in the high-velocity tail region. Determining why the electrostatic bursts begin to be seen continuously rather than in packets, how the electrons trapped in the potential well are accelerated, and how the trapped electrons escape is beyond the scope of the present paper. Several possible mechanisms were detailed by *Gurnett and Reinleitner* [1983], including change of phase velocity as the whistler mode wave propagates away from the generation region and dispersive acceleration.

As shown in Table 1, the whistler mode waves around 350 Hz on September 11, 1996, at ~0136 UT have a measured parallel phase velocity of ~3250 km s^{-1}. Interferometry data from a similar cusp TBL crossing on September 22, 1996, show that the velocity of the electrostatic bursts along **Bo** occurring in phase with a whistler mode wave of frequency ~300 Hz is ~3400 km s^{-1}. An electron with this velocity has a kinetic energy of 33 eV. Thus the six-channel waveform measurements are consistent with the interferometry measurements and with the electron measurements; that is, the whistler mode velocity is comparable to that of the electrons that the whistler mode wave traps, and to the velocity of the excited electrostatic bursts. Furthermore, from the Polar PWI interferometry waveform data we conclude that this velocity is consistent with that of the electron phase-space holes observed in the cusp on Polar, which were found to have velocities along **Bo** around 100–1000 km s^{-1} and parallel sizes of the order of a few hundred meters [*Franz*, 2000]. Inasmuch as the electrostatic

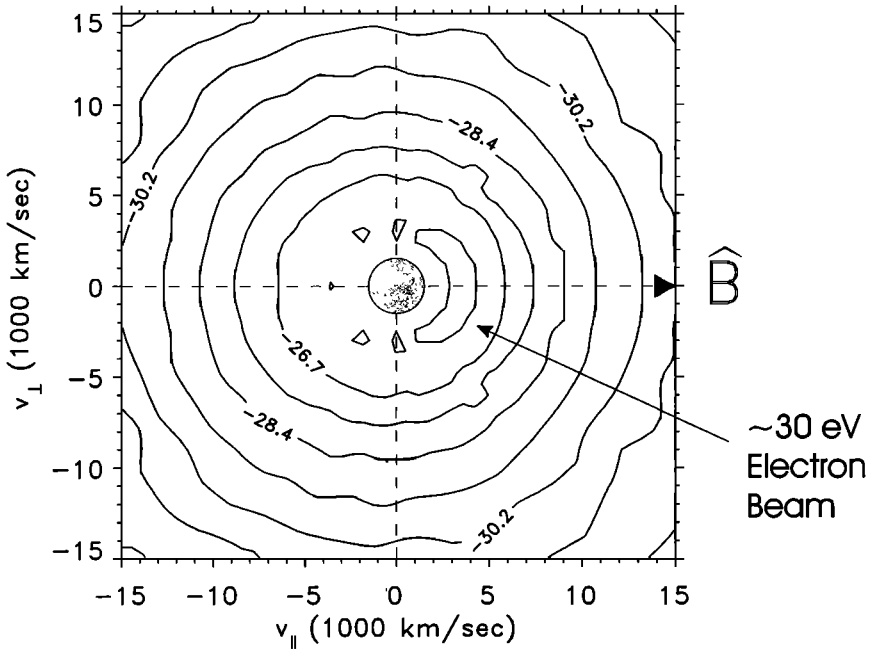

Figure 11. HYDRA contours of the electron distribution function in velocity space in units of s^3 cm^{-6}, showing an ~30 eV field-aligned electron beam. The distribution was obtained over a 13-s period that includes the time when high-frequency electrostatic bursts were observed to occur in packets at the frequency (350 Hz) of a simultaneously observed whistler mode wave (see Figure 4).

bursts discussed in this paper are observed to become unpacketized and steepen, it is intriguing to consider the possibility that the resistive medium instability, which is a modified two-stream instability, may be one mechanism whereby the electron phase-space holes are generated. *Goldman et al.* [1999] and *Muschietti et al.* [1999a, 1999b] have produced models in which the electron phase-space holes are generated through a two-stream instability.

Whether the electron phase-space holes observed in the Polar wave data in the cusp TBL are generated locally as a result of the resistive medium instability just discussed or whether they have propagated to this region is still under investigation. We note that it is highly probable that many of them have been created in regions of strong E-parallel, which is a characteristic of the reconnection layer and the bow shock. It is possible for them to propagate to the cusp TBL along the magnetic field lines that pass through the cusp. Because of the short timescales over which the pulses (indicative of these electron holes) are observed, they are thought to make up the high-frequency part of the broadband electrostatic noise observed along the magnetic field. The lower-frequency part of the broadband electrostatic noise is the subject of ongoing work, but Polar PWI observations tend to show that it is observed primarily perpendicular to the magnetic field. Although this noise may occasionally appear pulse-like in the time domain, it generally looks quite turbulent with timescales longer than that of the higher-frequency pulses, and it will create a broadband spectrum when transformed to the frequency domain by an FFT.

Finally, the electron cyclotron harmonic waves that are frequently observed in the cusp TBL are unusual in that they contain several electric field harmonics, as well as one or more magnetic field harmonics. We believe that these waves are generated locally in the cusp TBL, because they are nearly electrostatic (index of refraction <4) and therefore probably do not propagate, and because a significant electron anisotropy exists throughout the region that could lead to their generation [see *Menietti et al.*, 2001].

6. Summary

We have shown that magnetic noise extending from a few hertz up to the electron cyclotron frequency is present almost continuously throughout the cusp turbulent boundary layer. On the basis of previous studies [*Pickett et al.*, 1999b], we found that this noise is probably composed of more than one mode, i.e., whistler and Doppler-shifted kinetic Alfven wave modes. The source of this noise is believed to be the outflow region of the reconnection site closest to the spacecraft, which is a highly turbulent region in which whistler and Alfven modes are present [*Drake*, 1995]. We do not rule out the possibility, though, that the turbulence is generated as a result of the discontinuities at the edges of the TBL.

Broadband electrostatic noise from a few hertz to several kilohertz is also present in the cusp TBL, as well as prior to and after the cusp crossing. The broadband electrostatic noise observed in the frequency domain in many cases is the result of taking the FFT of a pulse in the time domain. These pulses occur of the order of hundreds of microseconds, are bipolar, and propagate along the magnetic field. On the basis of the work of *Franz et al.* [1998, 2000], *Mozer et al.* [1997], *Ergun et al.* [1998a, 1998b, 1998c], and *Tsurutani et al.* [1998, this issue] in various regions of the magnetosphere, we now know that these pulses indicate a detection of electron phase-space holes, rather than broadband plasma waves. These holes are most likely produced in regions of strong $E_{//}$ away from the cusp, although there is some indication that some of them may be

produced in the cusp TBL through the resistive medium instability.

We frequently observe bursts of electromagnetic whistler mode waves occurring on millisecond timescales around a few tens of hertz, a few hundreds of hertz, and just below the electron cyclotron frequency. The whistler mode wave bursts presented and discussed in this paper were shown to be inconsistent with generation through an electron cyclotron instability at the time and location of their detection, but this needs to be investigated in more detail, considering that the plasma may be warm. The most likely source for the generation of some of these whistler mode waves is at the X line where whistler mode dynamics drive magnetic reconnection [*Mandt et al.*, 1994; *Drake*, 1995], which may be bursty rather than steady, and in the process may create coherent whistler mode waves that propagate away from the reconnection site along reconnected field lines that pass through the cusp TBL. In addition, the whistler mode waves are observed propagating both toward and away from the Earth, which would be consistent with their generation at reconnection sites.

Electrostatic wave bursts that occur in packets modulated at the frequency of the whistler mode waves of a few hundred hertz are observed frequently in the cusp TBL. The few hundreds of Hz whistler mode waves have wave normal angles around 10°–20°, which means they have an electric field component along the magnetic field. We concluded from the example presented that 30-eV electrons were trapped and bunched by the parallel electric field of a whistler mode wave of phase velocity around 3250 km s^{-1} through Landau resonance. Each bunch of trapped electrons excited a burst of electrostatic noise via the resistive medium instability, which is a type of two-stream instability. This instability is characterized by a reduction in the electrostatic burst frequency below the electron plasma frequency (as observed) such that the burst may be broadband, downshifted Langmuir waves. However, more research needs to be done on these high-frequency electrostatic bursts in order to determine their exact nature and in particular to ascertain whether they can evolve (coalesce) into the electron phase-space holes that are seen by Polar PWI along the field lines in the cusp turbulent boundary layer.

Electron cyclotron harmonic waves are frequently observed in the cusp TBL. They have wave normal angles in the range of 80°–90° and both left- and right-hand polarizations. Although the fundamental frequency and one or more harmonics are sometimes observed in the magnetic field waveforms of these waves, the waves are nearly electrostatic. Thus they probably do not propagate and are generated locally in the TBL, probably through an electron temperature anisotropy.

Acknowledgments. This study was carried out under contract NAS5-30371 and grants NAG5-7943 and NAG5-2231 with NASA/Goddard Space Flight Center. The authors would first like to thank the reviewers for their extremely helpful comments and suggestions, most of which have been incorporated into the paper. The authors thank C. T. Russell for the use of the Polar MFE data, K. Ogilvie and the SWE Team for the use of the Wind/SWE data, R. Lepping for the use of the Wind/MFI data, J. Dowell of the Polar PWI Team at Iowa for developing most of the software used in analyzing the PWI data, NASA/GSFC for the use of the CDA Web plotting software, and R. Friedel of LANL and the Polar HYDRA programming team at Iowa for developing the PaPCo plotting package.

Janet G. Luhmann thanks the referees for their assistance in evaluating this paper.

References

Acuna, M. H., K. W. Ogilvie, D. N. Baker, S. A. Curtis, D. H. Fairfield, and W. H. Mish, The Global Geospace Science Program and its investigations, *Space Sci. Rev.*, *71*, 5, 1995.

Blecki, J., et al., ULF-ELFL-VLF-HF plasma wave observations in the polar cusp onboard high and low altitude satellites, in *New Perspectives of Collective Effects: Proceedings of the International Topical Conference on Plasma Physics: Trieste, Italy, November 10–14, 1997*, edited by P. K. Shukla, L. Stenflo, and R. Bingham, *Phys. Scr.*, *T75*, 159, 1998.

Cattell, C. A., J. Dombeck, J. Wygant, M. K. Hudson, F. S. Mozer, M. A. Temerin, W. K. Peterson, C. A. Kletzing, C. T. Russell, and R. F. Pfaff, Comparisons of Polar satellite observations of solitary wave velocities in the plasma sheet boundary and the high altitude cusp to those in the auroral zone, *Geophys. Res. Lett.*, *26*, 425, 1999.

D'Angelo, N., A. Bahnsen, and H. Rosenbauer, Wave and particle measurements at the polar cusp, *J. Geophys. Res.*, *79*, 3129, 1974.

Drake, J. F., Magnetic reconnection: A kinetic treatment, in *Physics of the Magnetopause*, *Geophys. Monogr. Ser.*, vol. 90, edited by P. Song, B. U. O. Sonnerup, and M. F. Thomsen, p. 155, AGU, Washington, D. C., 1995.

Ergun, R. E., et al., Fast satellite observations of electric field structures in the auroral zone, *Geophys. Res. Lett.*, *25*, 2025, 1998a.

Ergun, R. E., et al., Fast satellite observations of large-amplitude solitary structures, *Geophys. Res. Lett.*, *25*, 2041, 1998b.

Ergun, R. E., C. W. Carlson, J. P. McFadden, F. S. Mozer, L. Muschietti, I. Roth, and R. Strangeway, DeBye-scale plasma structures associated with magnetic-field-aligned electric fields, *Phys. Rev. Lett.*, *81*, 826, 1998c.

Franz, J. R., A study of electron phase-space holes in the polar magnetosphere, Ph.D. dissertation, Cornell Univ., Ithaca, N. Y., 2000.

Franz, J. R., P. M. Kintner, and J. S. Pickett, Polar observations of coherent electric field structures, *Geophys. Res. Lett.*, *25*, 1277, 1998.

Franz, J. R., P. M. Kintner, C. E. Seyler, J. S. Pickett, and J. D. Scudder, On the perpendicular scale of electron phase-space holes, *Geophys. Res. Lett.*, *27*, 169, 2000.

Gekelman, W., and R. L. Stenzel, Magnetic field line reconnection experiments, 6, Magnetic turbulence, *J. Geophys. Res.*, *89*, 2715, 1984.

Goldman, M. V., M. M. Oppenheim, and D. L. Newman, Nonlinear two-stream instabilities as an explanation for auroral bipolar wave structures, *Geophys. Res. Lett.*, *26*, 1821, 1999.

Gurnett, D. A., Auroral plasma waves, in *Auroral Physics*, edited by C.-I. Meng, M. J. Rycroft, and L. A. Frank, p. 241, Cambridge Univ. Press, New York, 1991.

Gurnett, D. A., and L. A. Frank, Plasma waves in the polar cusp: Observations from Hawkeye I, *J. Geophys. Res.*, *83*, 1447, 1978.

Gurnett, D. A., and L. A. Reinleitner, Electron acceleration by Landau resonance with whistler mode wave packets, *Geophys. Res. Lett.*, *10*, 603, 1983.

Gurnett, D. A., R. R. Anderson, B. T. Tsurutani, E. J. Smith, G. Paschmann, G. Haerendel, S. J. Bame, and C. T. Russell, Plasma wave turbulence at the magnetopause: Observations from ISEE 1 and 2, *J. Geophys. Res.*, *84*, 7043, 1979.

Gurnett, D. A., et al., The Polar plasma wave instrument, *Space Sci. Rev.*, *71*, 597, 1995.

Klimov, S. I., et al., Plasma waves using the BUDVAR complex for combined wave diagnostics (Prognoz-10-Interkosmos), *Cosmic Res., Engl. Transl.*, *24*, 143, 1986.

Kuznetsova, M. M., and L. M. Zelenyi, The theory of FTE: Stochastic percolation model in *Physics of Magnetic Flux Ropes*, *Geophys. Monogr. Ser.*, vol. 58, edited by C. T. Russell, E. R. Priest, and L. C. Lee, p. 473, AGU, Washington, D. C., 1990.

LaBelle, J., and P. Kintner, The measurement of wavelength in space plasmas, *Rev. Geophys.*, *27*, 495, 1989.

LaBelle, J., and R. A. Treumann, Plasma waves at the dayside magnetopause, *Space Sci. Rev.*, *47*, 175, 1988.

Mandt, M. E., R. E. Denton, and J. F. Drake, Transition to whistler mediated magnetic reconnection, *Geophys. Res. Lett.*, *21*, 73, 1994.

Menietti, J. D., J. S. Pickett, D. A. Gurnett, and J. D. Scudder, Electrostatic electron cyclotron waves observed by the plasma wave instrument on board Polar, *J. Geophys. Res.*, *106*, 6043, 2001.

Mozer, F. S., et al., New features of time domain electric-field structures in the auroral acceleration region, *Phys. Rev. Lett.*, *79*, 1281, 1997.

Muschietti, L., R. E. Ergun, I. Roth, and C. W. Carlson, Phase-space

electron holes along magnetic field lines, *Geophys. Res. Lett.*, *26*, 1093, 1999a.

Muschietti, L., I. Roth, R. E. Ergun, and C. W. Carlson, Analysis and simulation of BGK electron holes, *Nonlinear Proc. Geophys.*, *6*, 211, 1999b.

Pickett, J. S., et al., Plasma waves observed during cusp energetic particle events and their correlation with Polar and Akebono satellite and ground data, *Adv. Space Res.*, *24*(1), 23, 1999a.

Pickett, J. S., J. D. Menietti, J. H. Dowell, D. A. Gurnett, and J. D. Scudder, Polar spacecraft observations of the turbulent outer cusp/magnetopause boundary layer of Earth, *Nonlinear Proc. Geophys.*, *6*, 195, 1999b.

Reinleitner, L. A., D. A. Gurnett, and T. E. Eastman, Electrostatic bursts generated by electrons in Landau resonance with whistler mode chorus, *J. Geophys. Res.*, *88*, 3079, 1983.

Russell, C. T., The polar cusp, *Adv. Space. Res.*, *25*(7/8), 1413, 2000.

Russell, C. T., R. C. Snare, J. D. Means, D. Pierce, D. Dearborn, M. Larson, G. Bar, and G. Le, The GGS/Polar Magnetic Fields Investigation, *Space Sci. Rev.*, *71*, 563, 1995.

Savin, S. P., et al., Interball Tail Probe measurements in outer cusp and boundary layers, in *Geospace Mass and Energy Flow: Results From the International Solar-Terrestrial Physics Program*, *Geophys. Monogr. Ser.*, vol. 104, edited by J. L. Horwitz, D. L. Gallagher, and W. K. Peterson, p. 25, AGU, Washington, D. C., 1998a.

Savin, S. P., et al., The cusp/magnetosheath interface on May 29, 1996: Interball-1 and Polar observations, *Geophys. Res. Lett.*, *25*, 2963, 1998b.

Scudder, J., et al., HYDRA: A 3-dimensional electron and ion hot plasma instrument for the Polar spacecraft of the GGS mission, *Space Sci. Rev.*, *71*, 459, 1995.

Smith, E. J., and B. T. Tsurutani, Magnetosheath lion roars, *J. Geophys. Res.*, *81*, 2261, 1976.

Sonnerup, B. U. O., and L. J. Cahill Jr., Magnetopause structure and attitude for Explorer 12 observations, *J. Geophys. Res.*, *72*, 171, 1967.

Stix, T. H., *Waves in Plasmas*, Am. Inst. of Phys., New York, 1992.

Thorne, R. M., and B. T. Tsurutani, The generation mechanism for magnetosheath lion roars, *Nature*, *293*, 384, 1981.

Tsurutani, B. T., and G. S. Lakhina, Some basic concepts of wave-particle interactions in collisionless plasmas, *Rev. Geophys.*, *35*, 491, 1997.

Tsurutani, B. T., J. K. Arballo, G. S. Lakhina, C. M. Ho, B. Buti, J. S. Pickett, and D. A. Gurnett, Plasma waves in the dayside polar cap boundary layer: Bipolar and monopolar electric pulses and whistler mode waves, *Geophys. Res. Lett.*, *25*, 4117, 1998.

Tsurutani, B. T., J. K. Arballo, C. Galvan, X.-Y. Zhou, G. S. Lakhina, T. Hada, W. D. Gonzalez, and J. S. Pickett, Polar cap boundary layer waves: An auroral zone phenomenon, *J. Geophys. Res.*, this issue.

Zhou, X.-W., C. T. Russell, G. Le, S. A. Fuselier, and J. D. Scudder, The polar cusp location and its dependence on dipole tilt, *Geophys. Res. Lett.*, *26*, 429, 1999.

R. M. Braunger, D. A. Gurnett, G. B. Hospodarsky, W. S. Kurth, J. D. Menietti, J. S. Pickett, and J. D. Scudder, Department of Physics and Astronomy, University of Iowa, Iowa City, IA 52242-1942. (pickett@uiowa.edu)

J. R. Franz and P. M. Kintner, School of Electrical Engineering, Cornell University, Ithaca, NY 14853.

(Received May 2, 2000; revised November 14, 2000;
accepted November 14, 2000.)